Metallomics

Accepted Manuscript

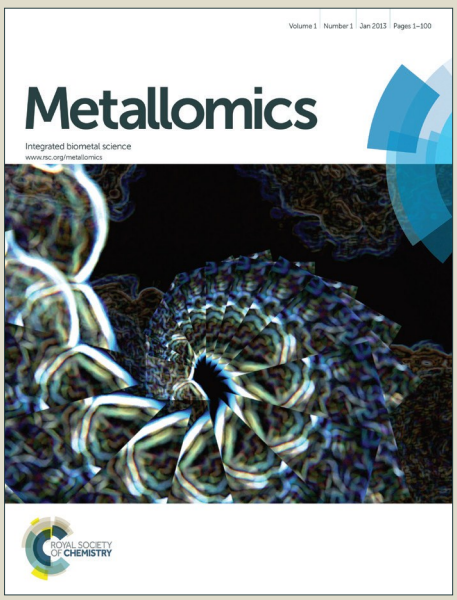

ROYAL SOCIETY OF CHEMISTRY

www.rsc.org/metallomics

Size- and surface chemistry-dependent pharmacokinetics and tumor accumulation of engineered gold nanoparticles after intravenous administration

Jing Wang[1,#], Ru Bai[1,#], Ru Yang[1,2], Jing Liu[1], Jinglong Tang[1], Ying Liu[1], Jiayang Li[1], Zhifang Chai[3], Chunying Chen[1, 3*]

[1] CAS Key Laboratory for Biomedical Effects of Nanomaterials and Nanosafety, National Center for Nanoscience and Technology, Beijing 100190, China

[2] College of Veterinary Medicine, China Agriculture University, Beijing 100193, China

[3] School for Radiological and interdisciplinary Sciences (RAD-X) & Collaborative Innovation Center of Radiation Medicine of Jiangsu Higher Education Institutions, Soochow University, Suzhou, China

Correspondence Email: chenchy@nanoctr.cn

Tel: 86-10-8254-5560; Fax: 86-10-6265-6765

Author Contributions: [#] These authors contributed equally.

Abstract

Engineered gold nanoparticles (AuNPs) have recently drawn an increased interest in disease diagnostics and therapies. However, reports on detailed studies of AuNPs regarding pharmacodynamics, pharmacokinetics, biodistribution, metabolism and toxicity potential are limited. It is common knowledge that *in vivo* behavior and fate of various AuNPs are influenced by their surface and size. However, comprehensive description and understanding of all variables are crucial for their further development toward potential clinical use. In this article, we describe the pharmacokinetics and biodistribution of mesoporous silica-coated gold nanorods functionalized with polyethylene glycol or bovine serum albumin (AuNR@SiO_2-PEG and AuNR@SiO_2-BSA, respectively) in tumor-bearing balb/c mice. To gain further insight on pharmacokinetics, biodistribution and tumor uptake, we also compare the results with BSA functionalized gold nanorods (AuNR-BSA) and gold clusters (AuNC-BSA). The results reveal that AuNR@SiO_2-PEG had longest blood half-life and the maximum percentage content in the tumor at 24 h and 3 days compared to other AuNPs. AuNR@SiO_2-PEG, AuNR@SiO_2-BSA and AuNR-BSA had primarily accumulated in the liver and spleen without apparent metabolism after 3 days, while the content of AuNC-BSA in the liver, spleen and kidney had obvious decrease, indicating a size-dependent metabolism process. Our results demonstrate how to manipulate the size and surface chemistry of AuNPs to prolong their blood circulation time, improve delivery into target organs and achieve a safer design of nanomedicines.

Keywords pharmacokinetics, biodistribution, tumor accumulation, gold nanoparticles, ICP-MS

Introduction

Due to their unique physicochemical properties, nanoscale devices and systems have great potential in biomedical applications, especially for disease diagnostics and therapies.[1-3] Compared to small molecular drugs and probes, nano-enabled drug delivery systems show many advantages, such as improved solubility, controlled release behavior and higher accumulation in cancerous lesions.[4] Recently, gold nanoparticles (AuNPs) engineered with different surface modification, size and shape have been proposed for use in multimodal imaging, local hyperthermia and targeted drug delivery.[5-7] However, detailed reports on elucidating the pharmacodynamics, pharmacokinetics, and toxicity potential of these AuNPs are very limited, even though they are very important before moving to their clinical trials.[8-10] Especially the pharmacokinetics and biodistribution results are prerequisites for the specific applications of nanomedicines and for the comprehensive risk assessment. Targeted delivery to solid tumors is one of the most challenging problems in cancer therapy. Unfortunately, detailed delivery mechanisms and design principles of nanomedicines are still not well understood.[11, 12]

Rapid expansion of nanoparticle research demands powerful technologies that provide accurate results of characterization and detection to better interpret experimental data and assist in rational design of future nanomedicines. Inductively coupled plasma mass spectrometry (ICP-MS) is a powerful analytical technique for elemental analysis because of its high sensitivity, low limit of detection, wide linear range and coincident multi-element measurement capability.[13] It provides an accurate and quantitative method to determine the metal content of nanoparticles. Our group reported a sensitive and accurate analytical method for quantitative determination of metallic impurities in carbon nanotubes combining the neutron activation technique and ICP-MS approach.[14, 15] Studies also show that metal particles could be mobilized from carbon nanotubes into the environment, and the amount of metal residues impacts the cell viability.[16] ICP-MS also serves as an effective tool to study pharmacokinetics, biodistribution, accumulation and metabolism of metal nanoparticles or metal ion doped nanoparticles in specific organs.[17] Size and surface chemistry are important factors influencing the *in vivo* behavior of nanoparticles including pharmacokinetics, biodistribution, tissue uptake and toxicity.[9, 17-22] De Jong et al. utilized ICP-MS to study the tissue distribution of spherical AuNPs as the function of particle size in rat.[21] The results revealed that d=10 nm AuNPs were present in the blood, liver, spleen, kidney, testis, thymus, heart, lung and brain, while the larger AuNPs (d=50, 100, 250 nm) were almost solely distributed in the blood, liver and spleen. Arvizo et al. has found that neutral and zwitterionic AuNPs showed longer blood circulation time whereas negatively and positively charged AuNPs displayed relatively short blood half-lives.[9] These pharmacological characteristics of AuNPs reflected on the tumor uptake, with enhanced tumor accumulation for neutral and zwitterionic AuNPs. Liu et al. observed that d=2.5 nm glutathione-coated gold nanoclusters exhibited faster tumor accumulation and better tumor targeting efficacy than the 20-100 nm of polyethylene glycol (PEG) coated AuNPs.[22] The better targeting specificity of glutathione-coated gold nanoclusters was mainly attributed to their smaller sizes compared to PEG-coated AuNPs, which helped them evade the reticuloendothelial system capture.

Gold nanorods (AuNRs) are responsive to near-infrared (NIR, 650-900 nm) light, and have been

widely researched as multifunctional theranostic agents.[23-25] AuNRs are prepared by wet chemical seed-mediated synthesis which usually uses cetyltrimethylammonium bromide (CTAB) as a structure-directing surfactant. However, CTAB is known to disrupt cell membrane integrity that results in cytotoxicity.[26] This toxicity of AuNR@CTAB systems can be reduced by the surface functionalization of AuNRs with PEG, serum protein or polyelectrolyte etc..[27, 28] To reduce the CTAB toxicity and improve the drug loading, we have developed mesoporous silica-coated AuNRs (AuNR@SiO_2) as a multifunctional cancer theranostic platform, capable of *in vitro* two-photon luminescence imaging, NIR light-controllable drug delivery, and hyperthermia.[29] Shen et al. demonstrated that AuNR@SiO_2 can simultaneously delivery heat and drugs to the tumor *in vivo*.[30] Recently, Ju et al. conjugated AuNR@SiO_2 with an aptamer that binds cytochrome C specifically for mitochondria-targeted chemo-photothermal therapy.[31] Xia et al. incorporated CdSe/ZnS quantum dots into AuNR@SiO_2 and also covalently conjugated folic acid as a targeting moiety to the surface of AuNR@SiO_2 for X-ray computed tomography and fluorescence imaging.[32] However, to date, there has been no detailed study on the pharmacokinetics and biodistribution of AuNR@SiO_2, which is very important for designing and optimizing nanomedicines for efficient and safe therapeutic purposes. Herein, in this article we carried out the pharmacokinetics and biodistribution studies of AuNR@SiO_2 with the functionalization of PEG (AuNR@SiO_2-PEG) and bovine serum albumin (AuNR@SiO_2-BSA), respectively. PEG and BSA make AuNR@SiO_2 more stable in the complex biological system. To gain further insight on pharmacokinetics, biodistribution and tumor uptake, we also compare the results with BSA functionalized AuNRs (AuNR-BSA) and gold clusters (AuNC-BSA).

Experimental

Reagents and materials

Hydrogen tetrachloroaurate (III) trihydrate ($HAuCl_4 \cdot 3H_2O$, 99.9%), silver nitrate ($AgNO_3$, 99%), ascorbic acid (AA, 99%), sodium borohydride ($NaBH_4$), cetyltrimethylammonium bromide (CTAB) were purchased from Alfa Aesar, United States. Tetraethyl orthosilicate (TEOS) and (3-mercaptopropyl)trimethoxysilan (97%) were purchased from Sigma-Aldrich, United States. Bovine serum albumin was purchased from AMERCO, United States. Maleimide functionalized polyethylene glycol (Mn=2000 Da) was purchased from Beijing JenKem Technology Limited Company, China. HNO_3 (MOS), H_2O_2 (MOS), hydrochloric acid (HCl, GR 36.0-38.0%) and sodium hydroxide were purchased from Beijing Chemical Reagent Institute, China. All the chemicals used were of analytical grade unless otherwise stated. Stock standard solutions for gold and bismuth element were obtained as 1,000 mg/L from the National Research Centre for CRMs, China. Ultrapure Milli-Q water with resistivity of 18.2 MΩ was used in all the experiments.

Apparatus

Electron microscopy images were obtained on a FEI Tecnai G2 F20 U-TWIN transmission electron microscope (TEM, FEI Company, USA). Hydrodynamic diameter and Zeta-potential were measured by a Malvern Zeta sizer Nano ZS instrument (Malvern Instruments, United Kingdom). Absorption spectra and fluorescence spectrum were acquired by a Tecan Infinite M200 spectrophotometer (Tecan Group, Switzerland). The amount of Au element was measured by an Elan DRC II inductively coupled plasma mass spectrometer (ICP-MS, Perkin-Elmer, USA). Serum biochemical analysis was performed by a biochemical autoanalyzer (Hitachi 7170, Japan).

The pathological sections were observed using an optical microscope (Nikon U−III Multipoint Sensor System, USA).

Synthesis of gold nanoparticles

AuNRs and AuNR@SiO_2 were synthesized as described in our previous work.[29] PEG-capped AuNR@SiO_2 was prepared in two steps. First, sulfhydryl functionalized AuNR@SiO_2 was obtained by adding 25 μL of 20 % of (3-mercaptopropyl)trimethoxysilan dissolved in the methanol to 10 mL of AuNR@SiO_2 aqueous solution. After stirring for 5 hours, the solution was centrifuged to remove the unreacted (3-mercaptopropyl)trimethoxysilan and resuspended in 2.5 mL of water. Then 2.5 mL of 2 mg/mL of maleimide functionalized PEG (Mn=2000 Da) was added to the Au@SiO_2-SH solution. The mixture was stirred overnight. BSA-capped AuNR@SiO_2 was obtained by using 0.5 wt% of BSA aqueous solution to resuspend AuNR@SiO_2 precipitation after centrifugation. The solution was stirred overnight. BSA-capped AuNR was prepared by adding AuNR aqueous solution dropwise into 0.5 wt% of BSA aqueous solution and stirred for three hours. BSA-capped AuNC was synthesized according to our previous published procedure.[33] Briefly, AuNC-BSA was obtained by adding 2.5 mL of 10 mM of $HAuCl_4$ aqueous solution to 2.5 mL of 30 mg/mL BSA aqueous solution. After stirring for 5 minutes at 37 ℃, 0.25 mL of NaOH (1 M) aqueous solution was added to the mixed solution. Then the mixture was incubated at 37 ℃ for 12 h. AuNC-BSA was further purified by dialysis in triple distilled water.

Characterization methods

The morphology and size of AuNPs were observed by TEM. Hydrodynamic diameter and Zeta-potential were measured in aqueous solution at 25 ℃ by a Malvern particle analyzer. The absorption spectra of AuNPs with the same gold concentration were obtained by Tecan Infinite M200 spectrophotometer with wavelength range from 400 nm to 1000 nm. The fluorescence emission spectrum of AuNC-BSA was measured by Tecan Infinite M200 spectrophotometer with 395 nm excitation wavelength.

Calibration and detection limit measurement of ICP-MS

To obtain a standard curve, a series of gold standard solutions (0.1, 0.5, 1, 5, 10, 50, 100 ng/mL) were prepared with the mixed acid solution containing 2 % of HNO_3 and 1 % of HCl and measured by ICP-MS for three times. Bismuth (20 ng/mL) in the mixed acid solution was used as an internal standard correction. The standard curve was obtained by the linear relation of mean counts per second against concentration of gold standard solutions. The limit of detection of the method, defined as three times of the standard deviation of reagent blank signal intensity were measured in 11 runs by ICP-MS.

Recovery measurements of blood and liver samples by ICP-MS

Procedures involving mice were approved by the Institutional Animal Care and Use Committee (IACUC). Recoveries from blood and liver samples were measured by ICP-MS to evaluate the feasibility and accuracy of the method. The measuring method is as follows. 200 μL of 0.1 mg/mL of AuNR@SiO_2-PEG phosphate buffered saline (PBS) solution was intravenously injected in a male balb/c mouse (4-6 weeks, 20 g of body weight). Six portions of blood samples with the same 80 μL of volume and six portions of liver samples with the same 0.1 g of weight in one mouse

were collected after 1 h post administration. Then three portions of gold standard solutions including 154 ng of gold element each portion were added into three portions of blood samples, respectively. Three portions of gold standard solutions including 900 ng of gold element each portion were added into three portions of liver samples, respectively. Each sample had three replicates. For ICP-MS measurement, the above samples were pre-digested with 4.0 mL of concentrated HNO_3 overnight. Then they were mixed with 3.0 mL of H_2O_2 (30 %) and digested for 2 h in open conical flasks on a hot plate at 50-150 ℃ by gradually warming. When the residual volume decreased to about 1 mL, 2.5 mL of aqua regia (HNO_3: HCl=1:3) was added to continue the digestion until the solution volume decreased to about 0.5 mL. Finally, the remaining solution was cooled and diluted to 3.0 g on the balance with the mixed acid solution containing 2 % of HNO_3 and 1 % of HCl. Each digested sample was measured by ICP-MS for three times. The recovery is calculated as follows:

$$\text{Recovery (\%)} = (A_{measured} - B_{measured})/V_{added} * 100$$

$A_{measured}$ refers to the measured value of the sample containing the added standard solution. $B_{measured}$ refers to the measured value of the sample itself. V_{added} is the value of the added gold content into the sample.

Pharmacokinetic studies of gold nanoparticles by ICP-MS

200 μL of 0.1 mg/mL of AuNPs in PBS solution were intravenously injected in male BALB/c mice (4-6 weeks, 20 g of body weight). Blood samples (100 μL) were collected at 1 min, 3 min, 5 min, 10 min, 30 min, 1h, 2 h, 6 h, 12 h and 24 h post administration from three mice at each group, respectively. All the blood samples were stored at -80 ℃ before ICP-MS measurement. The digestion process was as described above. Each sample was measured by ICP-MS for three times. After the quantitative measurement by ICP-MS, the data was analyzed and evaluated. The pharmacokinetic data of the four kinds of AuNPs were fitted into the classical two-compartment pharmacokinetic model. The important kinetic parameters, such as absorption half-life ($t_{1/2\alpha}$), elimination half-life ($t_{1/2\beta}$), areas under the curve (AUC), plasma clearance (Cl) and apparent volume of distribution (V_d) were calculated.

Biodistribution studies of gold nanoparticles in tumor-bearing mice by ICP-MS

The hair on the right hind leg of the male balb/c mice (4-6 weeks, 20 g of body weight) was first removed by the clipper. Then $1*10^6$ murine 4T1 breast cancer cells were implanted at the right hind leg in the mice to prepare tumor-bearing mice. When the tumors reached about 0.5 mm^3, mice were given a tail-vein injection of 200 μL of PBS solution containing 0.1 mg/mL of AuNPs. The mice were sacrificed at 1 h, 24 h and 3 days, respectively. Each group had three mice as replicates. Tumor and other organs including the heart, liver, spleen, lung and kidneys were dissected and weighted. All the tissue samples were stored at -80 ℃ before ICP-MS measurement. The digestion and measurement process were as described above. Each digested tissue sample was measured by ICP-MS for three times.

Serum biochemical analysis

To evaluate the toxicity of the four kinds of AuNPs after 3 days post intravenous injection, serum biochemical analysis was carried out using a standard protocol. After standing at room temperature for 3 h, the whole blood was centrifuged at 3000 rpm for 15 min. Then, serum was

collected from the supernatant and examined by a biochemical autoanalyzer to explore the influence of AuNPs on the liver and kidney function. The liver function was evaluated with serum levels of alanine aminotransferase (ALT), aspartate aminotransferase (AST) and total bilirubin level (TBIL). The kidney function was evaluated with serum levels of creatinine (CREA), uric acid (UA) and blood urea nitrogen (BUN).

Histopathological examination

The tissues (heart, liver, spleen, lung and kidney) of the mice after 3 days post intravenous injection were harvested and fixed in a 10 % of formalin solution. The histopathological tests were performed according to the standard laboratory procedures. Briefly, the tissue samples were embedded in paraffin blocks, sectioned into 5 μm of slices, and mounted onto the glass slides. After hematoxylin-eosin (H&E) staining, the sections were observed, and photos were taken using an optical microscope. (Magnification: heart, liver, spleen, lung and kidney × 20)

Results and discussion

Synthesis and characterization of gold nanoparticles

Four kinds of AuNPs with varied surface chemistry and size were synthesized, including AuNR@SiO_2-PEG, AuNR@SiO_2-BSA, AuNR-BSA and AuNC-BSA. TEM images of AuNR@SiO_2-PEG (Fig. 1a) and AuNR@SiO_2-BSA (Fig. 1b) show that AuNR@SiO_2 was around 110 nm in length and 70 nm in width. As shown in Figure 1c, AuNR had the aspect ratio of 4.0 with length of 60 nm and width of 15 nm. The TEM image of AuNC-BSA shows that the diameter of AuNC was around 2 nm (Fig. 1d). All the four kinds of AuNPs had uniform size and morphology with good dispersivity based on the TEM images. The hydrodynamic diameters measured by dynamic light scattering method were 41.8 nm for AuNR@SiO_2-PEG and 44.3 nm for AuNR@SiO_2-BSA, respectively (Table 1), implying that the two kinds of AuNPs had the similar size. The hydrodynamic diameter of AuNC-BSA was 7.2 nm (Table 1) which was much bigger than that in the TEM image (Fig. 1d, 2 nm), confirming the presence of BSA at the surface of AuNC. The hydrodynamic diameter of AuNR-BSA was 20.2 nm whose size was between AuNR@SiO_2-BSA and AuNC-BSA (Table 1). Zeta-potential results revealed the negative charges for AuNR@SiO_2-BSA, AuNR-BSA and AuNC-BSA (Table 1) due to the coating of different amounts of BSA. The Zeta-potential of AuNR@SiO_2-PEG was nearly zero because of the neutral PEG conjugation (Table 1). The absorption spectra of AuNR@SiO_2-PEG, AuNR@SiO_2-BSA and AuNR-BSA had similar longitudinal surface plasmon resonance (SPR) absorption peak around 800 nm demonstrating the good stability during the functionalization process of nanoparticles (Fig. 2a). As shown in Figure 2b, AuNC-BSA had an emission peak at 670 nm under 395 nm of excitation wavelength, revealing the successful preparation of AuNC.

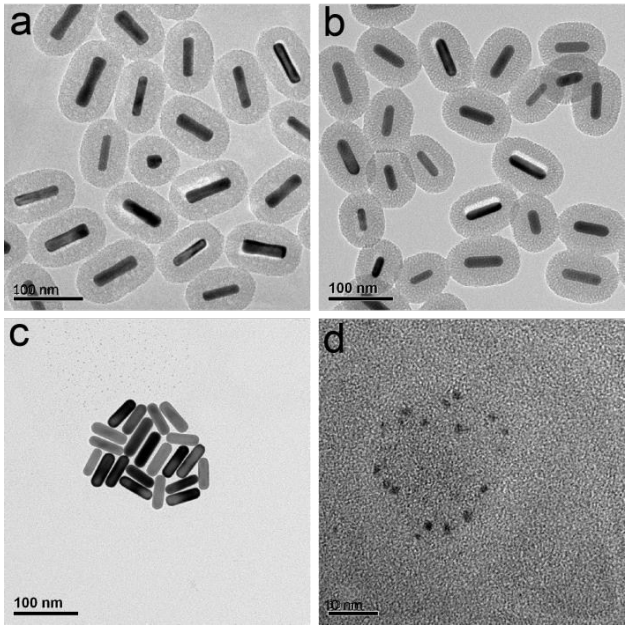

Fig. 1 TEM images of AuNR@SiO_2-PEG (a), AuNR@SiO_2-BSA (b), AuNR-BSA (c) and AuNC-BSA (d).

Table 1 Hydrodynamic diameters and Zeta-potentials of AuNPs.

	AuNR@SiO_2-PEG	AuNR@SiO_2-BSA	AuNR-BSA	AuNC-BSA
Z-Average (d. nm)	41.8	44.3	20.2	7.2
Zeta Potential (mV)	-0.06	-14.1	-19.5	-23.5

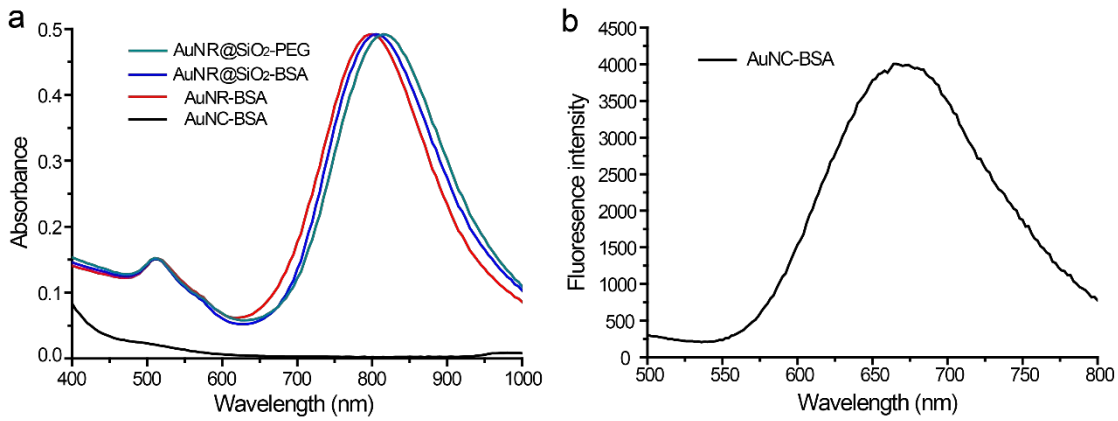

Fig. 2 Absorption spectra of AuNR@SiO_2-PEG, AuNR@SiO_2-BSA, AuNR-BSA and AuNC-BSA (a) and fluorescence emission spectrum of AuNC-BSA at 395 nm excitation wavelength (b).

Analytical performance of ICP-MS and recovery measurements

Under the optimized conditions, the analytical performance of the proposed ICP-MS method was evaluated. The linear range of gold element was measured between 0.1 ng/mL and 100 ng/mL

with a good correlation coefficient of 0.99995. According to the International Union of Pure and Applied Chemistry (IUPAC) definition, the limit of detection (LOD) of the method defined as three times the standard deviation of the entire procedural reagent blank, was 5.7 pg/mL for gold element in nanoparticles.

For the recovery measurements, we added 154 ng and 900 ng of the standards to the blood and liver samples, respectively. The recoveries of gold element were 91.5 % for the blood samples and 95.5 % for the liver samples, respectively, both of which were at satisfactory levels. The results indicated that the present method could be applied to the real samples.

Pharmacokinetic studies of gold nanoparticles by ICP-MS

The results of plasma drug concentration versus time curves show that the four kinds of AuNPs have obvious differences in pharmacokinetic profiles (Fig. 3a, b). AuNR@SiO_2-PEG had the longest blood circulation time followed by AuNC-BSA, while AuNR-BSA had the shortest one. All four kinds of AuNPs revealed a rapid initial concentration drop followed by more gradual decline. At 3 min, the percentage concentration of AuNR@SiO_2-PEG remained in the blood was 76.0 % and then dropped to 34.2 % after 1 h post administration, while the percentage concentration of the others at 3 min was 65.5 % (AuNC-BSA), 51.8 % (AuNR@SiO_2-BSA) and 5.0 % (AuNR-BSA), respectively, and dropped to 10.7 % (AuNC-BSA), 2.3 % (AuNR@SiO_2-BSA) and 0.3 % (AuNR-BSA), respectively, after 1 h post administration.

The pharmacokinetic data of the four AuNPs were fitted into the classical two-compartment model. The main pharmacokinetic parameters are listed in Table 2. Functionalization of AuNR with mesoporous silica (AuNR@SiO_2-BSA: $t_{1/2\alpha}$=3.3 min) enhanced the blood circulation time of AuNRs ($t_{1/2\alpha}$=34 s). After the conjugation of PEG to the surface of mesoporous silica, the blood circulation time of AuNR@SiO_2-PEG ($t_{1/2\alpha}$=18.6 min) was further increased. The blood half-life of AuNR@SiO_2-PEG was much shorter than other PEG-functionalized AuNPs reported in the literature, such as that of PEG coated hollow gold nanospheres ($t_{1/2}$= 8.19 h)[10] and PEG coated AuNRs ($t_{1/2}$= 17 h)[34] which may be due to the differences of molecular weight and modified density of PEG chain.[35, 36] Perrault et al. reported that the blood half-life was 9.2 times improvement when d=67 nm of AuNPs was functionalized with 5 kDa PEG ($t_{1/2}$= 9.2 h) compared to AuNPs with 2 kDa PEG ($t_{1/2}$= 1.0 h).[35] Meanwhile, the blood half-life of d=87 nm of AuNPs with 5 kDa PEG ($t_{1/2}$= 3.3 h) was also much shorter than those of d=67 nm of AuNPs with 5 kDa PEG ($t_{1/2}$= 9.2 h) because the bigger size of the nanoparticle offered lower surface PEG density.[35] Higher PEG molecular weight or higher PEG density can markedly decrease the serum protein adsorption and phagocytic uptake, thus showing prolonged blood circulation time.[8] In this article, AuNR@SiO_2-PEG was prepared by conjugating PEG on the surface of mesoporous silica and thus had relatively low PEG modified density. Besides, the molecular weight of PEG is 2 kDa which is relatively low. Thus it is not strange that the half-life of AuNR@SiO_2-PEG was shorter than some PEG functionalized AuNPs reported in the literature.

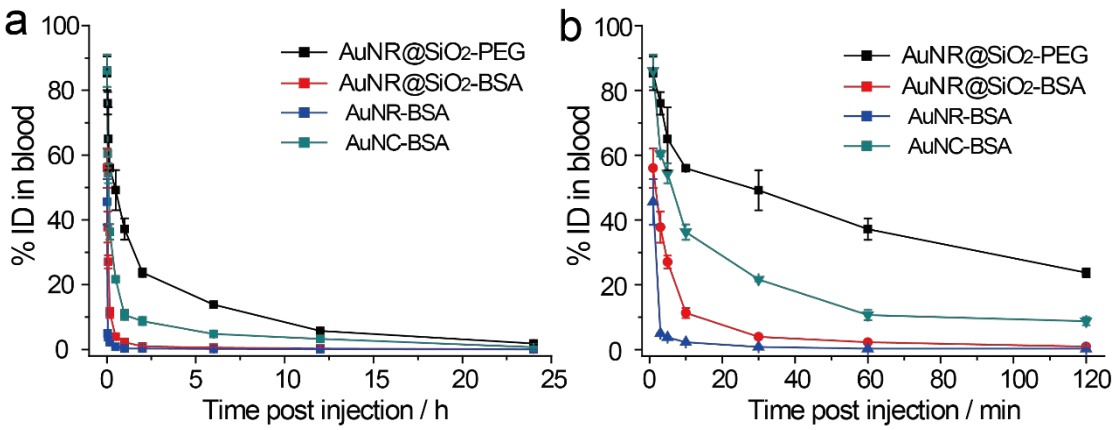

Fig. 3 *In vivo* pharmacokinetic data of AuNR@SiO_2-PEG, AuNR@SiO_2-BSA, AuNR-BSA and AuNC-BSA measured by ICP-MS following intravenous administration. (a) Blood concentration-time curves at 1 min, 3 min, 5 min, 10 min, 1 h, 2 h, 6 h, 12 h and 24 h. (Data is expressed as the percentage of the injected dose (% ID)). (b) Blood concentration-time curves within 2 h. Each group has three mice as replicates.

The pharmacokinetic data also revealed that AuNR@SiO_2-PEG was eliminated more slowly from the bloodstream ($t_{1/2\beta}$=6.32 h, Cl=0.48 mL/h) than AuNR@SiO_2-BSA ($t_{1/2\beta}$=0.75 h, Cl=9.30 mL/h) due to the longer elimination half-life and lower value of plasma clearance. The value of AUC of AuNR@SiO_2-PEG (41.24 μg/mL*h) markedly increased by about 19-fold in comparison to that of AuNR@SiO_2-BSA (2.15 μg/mL*h), also illustrating that the blood half-life of AuNR@SiO_2-PEG was longer than AuNR@SiO_2-BSA. The large V_d values of the four kinds of AuNPs were far beyond the volume of the mice's body fluid, which implies that AuNPs must accumulate in the organ tissues. The smaller V_d value of AuNR@SiO_2-PEG (V_d: 4.43 mL) than Au@SiO_2-BSA (V_d: 10.02 mL) meant that more AuNR@SiO_2-PEG were in the blood in accord with their longer plasma half-life. Our results were consistent with the previous report that when a drug formulation shows prolonged blood half-life, an increased $t_{1/2}$, a reduced Cl, an increased AUC and a reduced V_d are observed.[8]

To gain more insight into the details of pharmacokinetics, we also compare the results of AuNR@SiO_2-BSA with AuNR-BSA and AuNC-BSA. It can be clearly seen that AuNC-BSA of smaller size (d< 10 nm) had longer blood circulation time ($t_{1/2\alpha}$=6.1 min) than AuNR@SiO_2-BSA ($t_{1/2\alpha}$=3.3 min) and AuNR-BSA ($t_{1/2\alpha}$=34 s). Besides, AuNC-BSA also had the slowest blood clearance, the highest AUC value and the smallest V_d value compared to AuNR@SiO_2-BSA and AuNR-BSA.

Table 2 Pharmacokinetic parameters of AuNR@SiO_2-PEG, AuNR@SiO_2-BSA, AuNR-BSA and AuNC-BSA

	AuNR@SiO_2-PEG	AuNR@SiO_2-BSA	AuNR-BSA	AuNC-BSA
$t_{1/2\alpha}$	18.6 min	3.3 min	34 s	6.1 min
$t_{1/2\beta}$	6.32 h	0.75 h	0.20 h	6.14 h
AUC	41.24 μg/mL*h	2.15 μg/mL*h	0.44 μg/mL*h	17.89 μg/mL*h
Cl	0.48 mL/h	9.30 mL/h	45.45 mL/h	1.12 mL/h
V_d	4.43 mL	10.02 mL	13.35 mL	9.90 mL

Biodistribution studies of gold nanoparticles in tumor-bearing mice by ICP-MS

The biodistribution results show that AuNR@SiO_2-PEG, AuNR@SiO_2-BSA and AuNR-BSA were mainly accumulated in the liver (70 %~ 75% of the injected dose at 24 h) and spleen (5 %~11 % of the injected dose at 24 h) and small amounts accumulated in the tumor, kidney, lung and heart (Fig. 4a-f). In addition to the main accumulation sites of the liver and spleen, AuNC-BSA also had more accumulation in the kidney (5.42 % of the injected dose at 1 h) with significant differences ($P<0.01$) compared to other three kinds of AuNPs (Fig. 4d).

Effective accumulation in the tumor site determines the detection sensitivity and therapeutic efficacy of theranostic agents. For the tumor accumulation, AuNR@SiO_2-PEG had the maximum of 0.83 % of the injected dose in the tumor at 24 h compared to other AuNPs followed by AuNC-BSA (0.61 % in the tumor at 24 h) which is coincident with previous reports that the longer plasma half-life led to more accumulation in the tumor (Fig. 4a).[9, 35] It is worth noting that AuNC-BSA had faster accumulation in the tumor than other AuNPs at 1 h (Fig. 4a). Besides, all AuNPs first gradually accumulated in the tumor then the excretion process took over at 3 days, implying that there is an optimal treatment window for better therapeutic efficacy and reduced side effects when using AuNPs as photothermal carriers. From our results, due to the higher content of AuNPs in the tumor, the time of 24 h post intravenous injection is more suitable than 1 h and 3 days for the NIR laser irradiation to conduct photothermal therapy.

All AuNPs had rapid and massive accumulation in the liver (about 70 % of the injected dose at 1 h, Fig. 4b). Of note, AuNR@SiO_2-PEG, AuNR@SiO_2-BSA and AuNR-BSA had accumulated in the liver without obvious decrease after 3 days, while the content of AuNC-BSA in the liver decreased to about 47% after 3 days with significant differences ($P<0.01$) compared to other AuNPs (Fig. 4b). The four kinds of AuNPs had increased accumulation in the spleen after 24 h then slight decrease after 3 days (Fig. 4c). The total amount of AuNR@SiO_2-PEG (8.6 % at 24 h) and AuNC-BSA (4.8 % at 24 h) in the spleen were lower than the other two kinds of AuNPs (>10% at 24 h) with AuNC-BSA having the lowest total amount in the spleen. AuNC-BSA had massive accumulation in the kidney (more than other AuNPs) with significant differences ($P<0.01$) (Fig. 4d). After 3 days, nearly half of AuNC-BSA could metabolize from the kidney, indicating a size-dependent renal clearance due to the fact that the physical size of glomerular filtration is approximately 8 nm.[33] Besides, AuNR@SiO_2-PEG had more accumulation in the kidney than AuNR@SiO_2-BSA and AuNR-BSA with significant differences ($P<0.01$) at 1 h and 24 h (Fig. 4d).

Interestingly, all AuNPs showed a gradual decline process both in the lung and heart from 1 h to 3 days (Fig. 4e, f). AuNR@SiO_2-PEG and AuNR@SiO_2-BSA had higher accumulation in the lung than AuNR-BSA and AuNC-BSA at 1 h and 24 h (Fig. 4e). AuNC-BSA had more accumulation in the heart than other AuNPs with significant differences ($P<0.01$) (Fig. 4f).

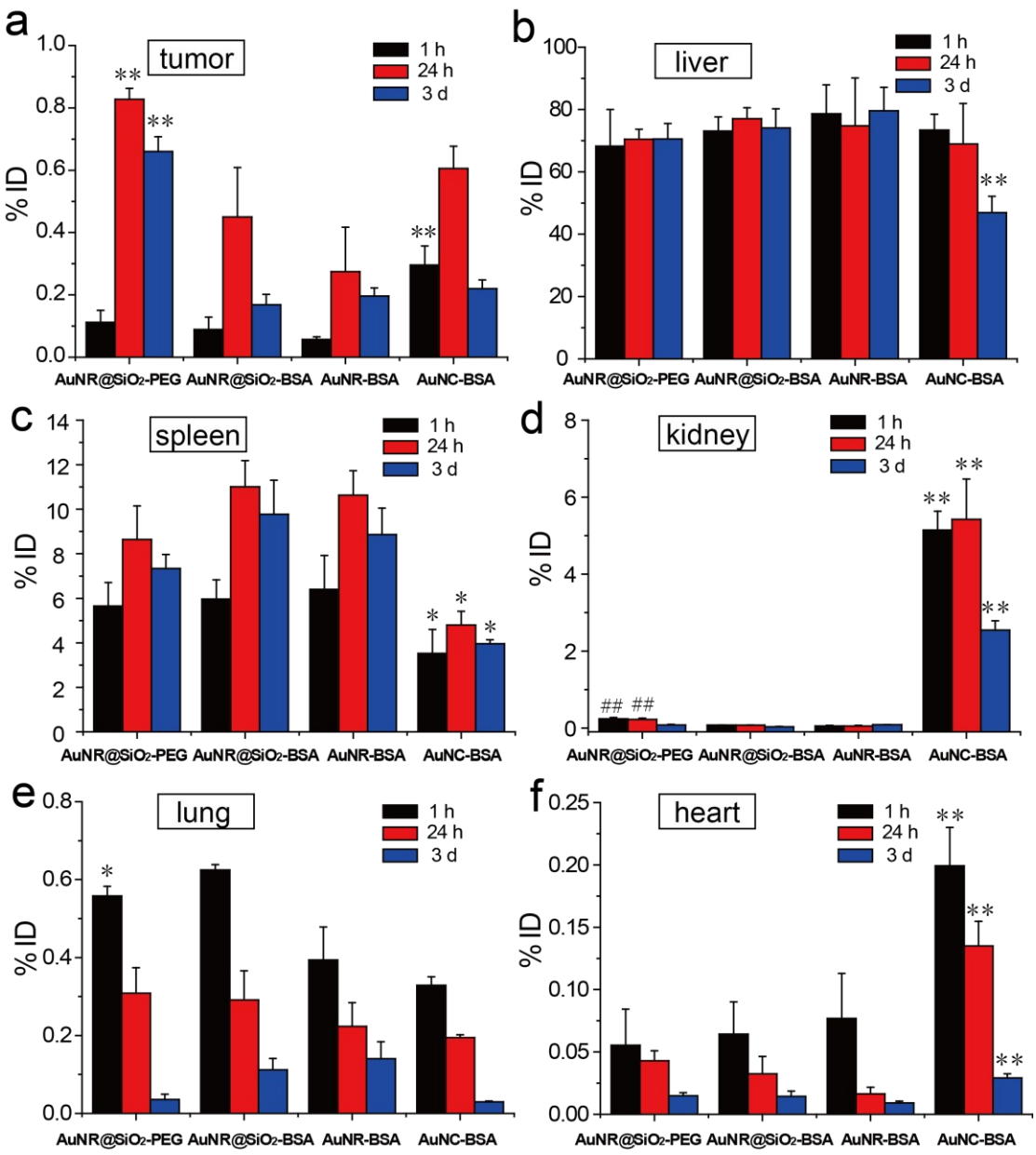

Fig. 4 Biodistribution of AuNPs by ICP-MS measurement after intravenous administration. (Data is expressed as % ID). The tumor (a), liver (b), spleen (c), kidney (d), lung (e) and heart (f) were dissected at 1 h, 24 h and 3 d after intravenous administration, respectively and measured by ICP-MS. Each group has three mice as replicates. (**$P<0.01$, *$P<0.05$, significant difference between the labeled AuNPs and other AuNPs at the corresponding time point; $^{\#\#}P<0.01$, significant difference between AuNR@SiO_2-PEG compared with AuNR@SiO_2-BSA and AuNR-BSA in the kidney.)

Although AuNR@SiO_2-PEG had longer blood half-life than other AuNPs, it was still largely distributed to the liver and spleen. The surface chemistry in our systems could effectively change the pharmacokinetics and tumor accumulation of nanoparticles, but it did not have obvious influence on biodistribution. However, there were great differences of pharmacokinetics and biodistribution for nanoparticles with small size (< 10 nm) and nanoparticles with relative big size (15~110 nm). Compared with AuNR@SiO_2-BSA and AuNR-BSA, AuNC-BSA with smaller size (< 10 nm) had the longest blood half-life, maximum uptake by the tumor and partial metabolism in the liver and kidney. Thus, size seems to be the dominating factor for *in vivo* biodistribution and metabolism when the nanoparticles are wrapped in BSA.

Toxicity evaluation by serum biochemical analysis and histopathological examination

Because AuNPs mainly accumulated in the liver, spleen and kidney, toxicity measurements of serum biochemical analysis and histopathological examination were conducted to evaluate their toxicity potential for major organs.

To test the acute toxicity of the AuNPs in tumor-bearing mice model, the liver function was evaluated with serum levels of ALT, AST and TBIL (Fig. 5a, b) and the kidney function was evaluated with serum levels of CREA, UA and BUN (Fig. 5b, c). Because the tumor itself may cause liver and kidney dysfunction, there were some differences between the normal control and tumor control. Our results demonstrated that all the groups injected with AuNPs showed no significant differences with the tumor control, suggesting that the four kinds of AuNPs could not cause acute liver and kidney dysfunction in mice under the dosage of 1 mg/kg body weight of Au element after 3 days post injection.

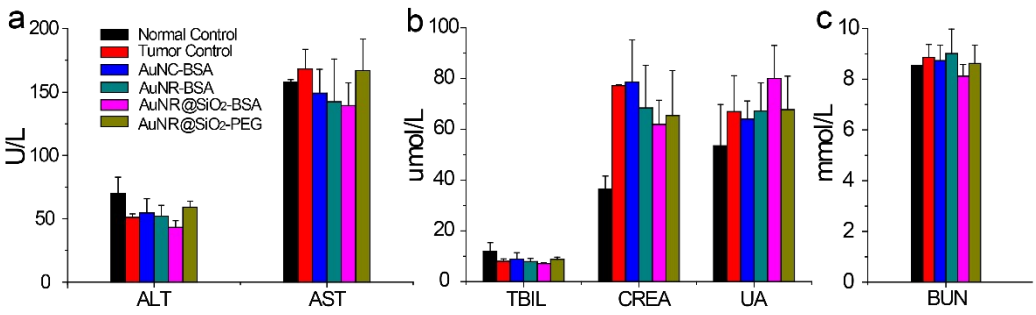

Fig. 5 Serum biochemical analysis of gold nanoparticles at 3 days post intravenous administration. ALT, AST (a) and TBIL (b) were examined to reveal the function of the liver; CREA, UA (b) and BUN (c) were examined to reveal the function of the kidney.

The histopathological examinations of the tissues (heart, liver, spleen, lung and kidney) of the mice after 3 days post injection was performed by the standard histological techniques with H&E staining. Comparing to the tumor control, there were no obvious pathological changes in the heart, liver, spleen, lung and kidney for the groups injected with AuNPs (Fig. 6). Because the 4T1 cells are highly malignant breast cancer cells, obvious metastases in the lung (red arrows indicate the metastases) were observed in the group of tumor control and the groups injected with AuNPs (Fig. 6).

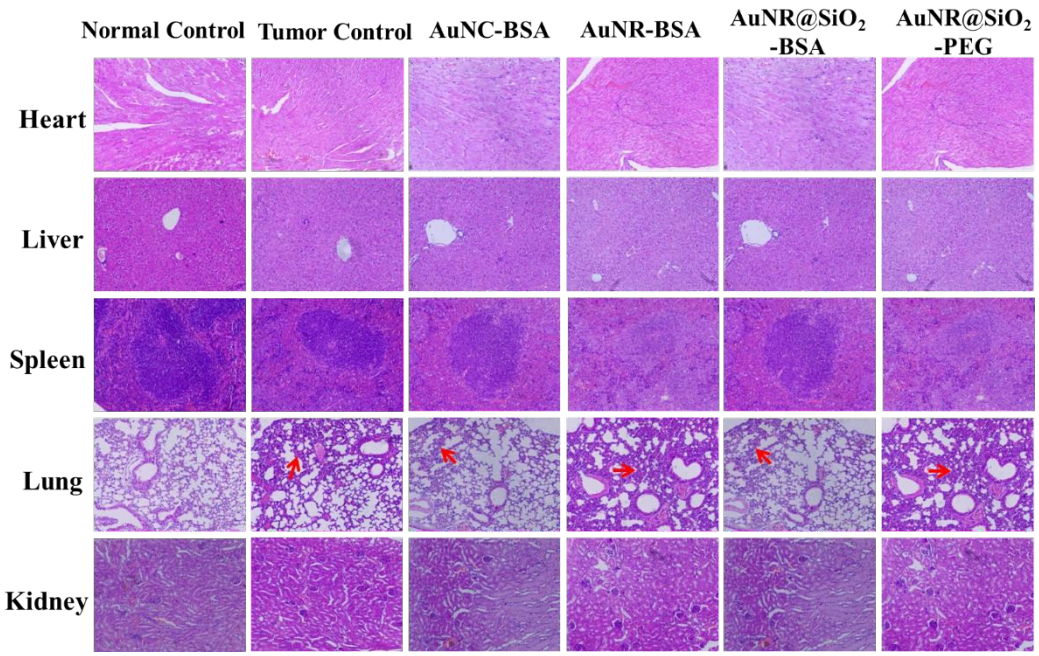

Fig. 6 Histopathological samples of the tissues (heart, liver, spleen, lung and kidney) of the mice after 3 days post injection. Red arrows indicate the metastases of the tumor in the lung. (Magnification: × 20)

Conclusion

Comprehensive description and understanding of *in vivo* behavior and fate of AuNPs are crucial for their implementation into the clinical setting. AuNPs with various surface functional attachments, shapes and sizes can also be used as ideal models to study the biological effects and biosafety of nanoparticles. In this article, we prepared four kinds of AuNPs with different surface coating or size and studied their pharmacokinetics and biodistribution in tumor-bearing mice model by ICP-MS. Our results reveal that AuNR@SiO_2-PEG had longest blood half-life and the maximum percentage content in the tumor both at 24 h and 3 days compared to other AuNPs followed by AuNC-BSA which is coincident with the previous reports that the longer plasma half-life led to more accumulation in the tumor. AuNR@SiO_2-PEG, AuNR@SiO_2-BSA and AuNR-BSA had primarily accumulated in the liver and spleen of the mice without apparent metabolism, while the content of AuNC-BSA in the liver, spleen and kidney of mice had obvious decrease after 3 days, indicating a size-dependent metabolism process. The surface chemistry and size in our systems can effectively change the pharmacokinetics and tumor accumulation of nanoparticles. Size seems to be the dominating factor for *in vivo* biodistribution and metabolism. By understanding the pharmacokinetics and biodistribution of nanoparticles at organism level, it will be possible to manipulate the surface chemistry and size of nanomedicines to prolong their blood circulation time, enhance delivery efficacy into target organs and finally achieve a safer design of nanomaterials.

Acknowledgements

This work was financially supported by the Ministry of Science and Technology of China (National Basic Research Programs: 2011CB933401 and 2012CB934003), International Science

& Technology Cooperation Program of China, Ministry of Science Technology of China (2013DFG32340 and 2014DFG52500), the National Science Fund for Distinguished Young Scholars (11425520) and the National Science Foundation of China (21320102003).

References

1 Z. J. Zhang, J. Wang and C. Y. Chen, *Adv. Mater.*, 2013, **25**, 3869.

2 D. Peer, J. M. Karp, S. Hong, O. C. FaroKhzad, R. Margalit and R. Langer, *Nat. Nanotechnol.*, 2007, **2**, 751.

3 M. Cao, X. R. Liu, J. B. Tang, M. H. Sui, Y. Q. Shen, *Sci. China Chem.*, 2014, **57**, 633.

4 R. Duncan, Nat. Rev. Cancer, 2006, 6, 688.

5 S. D. Huo, S. B. Jin, K. Y. Zheng, S. T. He, D. L. Wang, X. J. Liang, *Sci. Bull.*, 2013, **58**, 4072.

6 Z. Y. Ma, H. X. Xia, Y. P. Liu, B. Liu, W. Chen, Y. D. Zhao, *Sci. Bull.*, 2013, **58**, 2741.

7 E. Boisselier and D. Astruc, *Chem. Soc. Rev.*, 2009, **38**, 1759.

8 M. T. Zhu, S. Perrett and G. J. Nie, *Small*, 2013, **9**, 1619.

9 R. R. Arvizo, O. R. Miranda, D. F. Moyano, C. A. Walden, K. Giri, R. Bhattacharya, J. D. Robertson, V. M. Rotello, J. M. Reid and P. Mukherjee, *Plos One*, 2011, **6**, e24374.

10 J. You, J. Zhou, M. Zhou, Y. Liu, J. D. Robertson, D. Liang, C. Van Pelt and C. Li, *Part. Fibre Toxicol.*, 2014, **11**, 26.

11 P. Krystek, Microchem. J., 2012, 105, 39.

12 J. Deng, D. H. Yu, C. Y. Gao, *Sci. China Chem.*, 2013, **56**, 1533.

13 X. D. Jin and H. P. Zhu, *J. Anal. At. Spectrom.*, 2000, **15**, 747.

14 C. C. Ge, W. Li, Y. F. Li, B. Li, J. F. Du, Y. Qiu, Y. Liu, Y. X. Gao, Z. F. Chai and C. Y. Chen, *J. Nanosci. Nanotechno.*, 2011, **11**, 2389.

15 C. C. Ge, F. Lao, W. Li, Y. F. Li, C. Y. Chen, Y. Qiu, X. Y. Mao, B. Li, Z. F. Chai and Y. L. Zhao, *Anal. Chem.*, 2008, **80**, 9426.

16 C. C. Ge, Y. Li, J. J. Yin, Y. Liu, L. M. Wang, Y. L. Zhao and C. Y. Chen, *Npg Asia Mater.*, 2012, **4**, e32.

17 S. Fraga, A. Brandao, M. E. Soares, T. Morais, J. A. Duarte, L. Pereira, L. Soares, C. Neves, E. Pereira, M. D. Bastos and H. Carmo, *Nanomedicine*, 2014, **10**, 1757.

18 L. Balogh, S. S. Nigavekar, B. M. Nair, W. Lesniak, C. Zhang, L. Y. Sung, M. S. Kariapper, A. El-Jawahri, M. Llanes, B. Bolton, F. Mamou, W. Tan, A. Hutson, L. Minc and M. K. Khan, *Nanomedicine*, 2007, **3**, 281.

19 H. Yang, L. B. Du, X. Tian, Z. L. Fan, C. J. Sun, Y. Liu, J. A. Keelan and G. J. Nie, *Toxicol. Lett.*, 2014, **230**, 10.

20 S. Hirn, M. Semmler-Behnke, C. Schleh, A. Wenk, J. Lipka, M. Schaeffler, S. Takenaka, W. Moeller, G. Schmid, U. Simon and W. G. Kreyling, *Eur. J. Pharm. Biopharm.*, 2011, **77**, 407.

21 W. H. De Jong, W. I. Hagens, P. Krystek, M. C. Burger, A. J. Sips and R. E. Geertsma, *Biomaterials*, 2008, **29**, 1912.

22 J. B. Liu, M. X. Yu, C. Zhou, S. Y. Yang, X. H. Ning and J. Zheng, *J. Am. Chem. Soc.*, 2013, **135**, 4978.

23 Z. J. Zhang, J. Wang and C. Y. Chen, *Theranostics*, 2013, **3**, 223.

24 L. G. Xu, Y. Liu, Z. Y. Chen, W. Li, Y. Liu, L. M. Wang, Y. Liu, X. C. Wu, Y. L. Ji, Y. L. Zhao, L. Y. Ma, Y. M. Shao and C. Y. Chen, *Nano Lett.*, 2012, **12**, 2003.

25 Z. J. Zhang, J. Wang, X. Nie, T. Wen, Y. L. Ji, X. C. Wu, Y. L. Zhao and C. Y. Chen, *J. Am. Chem. Soc.*, 2014, **136**, 7317.

26 A. M. Alkilany, P. K. Nagaria, C. R. Hexel, T. J. Shaw, C. J. Murphy and M. D. Wyatt, *Small*, 2009, **5**, 701.

27 T. Niidome, M. Yamagata, Y. Okamoto, Y. Akiyama, H. Takahashi, T. Kawano, Y. Katayama and Y. Niidome, *J. Control. Release*, 2006, **114**, 343.

28 Y. Qiu, Y. Liu, L. M. Wang, L. G. Xu, R. Bai, Y. L. Ji, X. C. Wu, Y. L. Zhao, Y. F. Li and C. Y. Chen, *Biomaterials*, 2010, **31**, 7606.

29 Z. J. Zhang, L. M. Wang, J. Wang, X. M. Jiang, X. H. Li, Z. J. Hu, Y. L. Ji, X. C. Wu and C. Y. Chen, *Adv. Mater.*, 2012, **24**, 1418.

30 S. Shen, H. Y. Tang, X. T. Zhang, J. F. Ren, Z. Q. Pang, D. G. Wang, H. L. Gao, Y. Qian, X. G. Jiang and W. L. Yang, *Biomaterials*, 2013, **34**, 3150.

31 E. G. Ju, Z. H. Li, Z. Liu, J. S. Ren and X. G. Qu, *Acs Appl. Mater. Inter.*, 2014, **6**, 4364.

32 H. X. Xia, X. Q. Yang, J. T. Song, J. Chen, M. Z. Zhang, D. M. Yan, L. Zhang, M. Y. Qin, L. Y. Bai, Y. D. Zhao and Z. Y. Ma, *J. Mater. Chem. B*, 2014, **2**, 1945.

33 J. J. Zhang, X. Nie, Y. L. Ji, Y. Liu, X. C. Wu, C. Y. Chen and X. H. Fang, *J. Nanosci. Nanotechno.*, 2014, **14**, 4124.

34 G. von Maltzahn, J.-H. Park, A. Agrawal, N. K. Bandaru, S. K. Das, M. J. Sailor and S. N. Bhatia, *Cancer Res.*, 2009, **69**, 3892.

35 S. D. Perrault, C. Walkey, T. Jennings, H. C. Fischer and W. C. Chan, *Nano lett.*, 2009, **9**, 1909.

36 C. Fang, B. Shi, Y. Y. Pei, M. H. Hong, J. Wu and H. Z. Chen, *Eur. J Pharm. Sci.*, 2006, **27**, 27.

Table of Contents

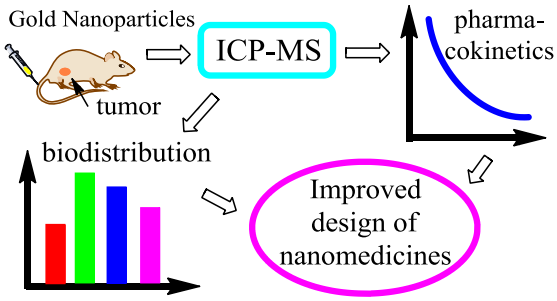

It is important and essential to study pharmacokinetics and biodistribution of gold nanoparticles for safer and more efficient therapeutic purposes.